Numerical Heat Transfer, Part B, 39:479–507, 2001

1040-7790/01 $12.00 + .00

FINITE-ELEMENT ANALYSIS OF INCOMPRESSIBLE NAVIER–STOKES EQUATIONS INVOLVING EXIT PRESSURE BOUNDARY CONDITIONS

S. F. Tsai and Tony W. H. Sheu
Department of Naval Architecture and Ocean Engineering, National Taiwan University, 73 Chow-Shan Road, Taipei, Taiwan, Republic of China

This article presents finite-element solutions for incompressible Navier–Stokes equations in velocity–pressure variables. Specific to this study is the inclusion of pressure boundary conditions into the mixed finite-element formulation. To provide an in-depth analysis of the finite-element model, rigorous derivations have been carried out. The justification for applying the finite-element code to simulate this class of flow problems is presented by solving a problem which is amenable to analytical solution and the backward-facing step benchmark problem. In addition, results for blood flow in a carotid artery are presented to show the applicability of the finite-element code to geometrically more complex problems.

1. INTRODUCTION

Incompressible viscous flow has been investigated rather intensively over the last few decades because of its wide range of industrial applications. Numerical study of this flow is also of theoretical importance to achieve the divergence-free constraint condition for the velocity vector in the calculation of equations of motion. The practical as well as theoretical importance of this flow has prompted us to work on this problem during the past few years. Numerical simulation of incompressible viscous flow entails several features which are troublesome to finite-element method (FEM) code development [1]. Aside from difficulties in satisfying the incompressibility constraint condition, avoiding convective instability [2], and reducing crosswind (false) diffusion errors [3], another issue that warrants further examination is proper specification of boundary conditions. The present study aimed to provide a theoretically rigorous approach to this issue. Under certain circumstances, boundary conditions other than the Dirichlet type for the velocity can be encountered. Typical examples are problems involving inflow or outflow boundaries, and the free surface. In the following, attention will be limited to the pressure boundary condition, which is often prescribed a priori at the outlet. Appropriate treatment of boundary con-

Received 28 January 2000; accepted 27 November 2000.
Financial support from the National Science Council of the Republic of China under grant NSC84-2212-E-002-060 is acknowledged.
Address correspondence to Prof. Tony W. H. Sheu, National Taiwan University, Department of Naval Architecture, 73 Chow-Shan Road, Taipei, Taiwan, Republic of China. E-mail: Tony.Sheu@cfd.na.ntu.edu.tw

NOMENCLATURE

a, b	coefficients shown in the linearized momentum equations	Re	Reynolds number ($\equiv \rho u_{\text{ref}} L_{\text{ref}} / \mu$)
$\mathbf{A}$	stiffness matrix	$\mathbf{u}$	velocity vector
B^i	upwinding part of the weighting function	W^i	weighting functions
		γ	Peclet number
$\mathbf{g}$	boundary velocity vector	Γ	boundary of Ω
h	height of the channel upstream of the backward-facing step	μ	dynamic viscosity of the fluid flow
H	height of the channel downstream of the backward-facing step	ρ	fluid density
		τ	intrinsic time scale
		Ω	physical domain
L	characteristic length		
N^i, M^i	shape functions	**Subscript**	
n	unit outward normal vector of Γ	ref	reference quantities
p	pressure		

ditions depends on the choice of working variables. This work addresses the use of the primitive variables $\mathbf{u}$ and p, which denote the velocity vector and pressure, respectively.

The rest of this article is organized as follows. In the next section, we present Navier–Stokes equations, which are written in terms of primitive variables. Equations of motion are solved together with the constraint condition to ensure the mass conservation. For the elliptic equations to be well posed, boundary conditions are prescribed. In Section 3, we present the weighted residual statement for the working equations subject to both Dirichlet and Neumann types of boundary conditions. The pressure prescribed a priori at the boundary is automatically accounted for via use of a divergence theorem. This is followed by introduction of the finite element used and the upwinding model applied to resolve pressure and velocity oscillations, respectively. In Section 4, we conduct a fundamental study of the Petrov–Galerkin finite-element model. In Section 5, we present an analytical proof of the pressure boundary condition prescribed and the finite-element code developed for simulation of incompressible Navier–Stokes equations. This is followed by calculation of the backward-facing-step problem, and hemodynamic study in carotid bifurcation. Finally, we draw conclusions in Section 6.

2. WORKING EQUATIONS

The motion of a viscous incompressible fluid flow in a simply connected domain Ω is governed by the Navier–Stokes equations cast in vector form:

$$\mathbf{u} \cdot \nabla \mathbf{u} + \nabla p - \frac{1}{\text{Re}} \nabla^2 \mathbf{u} = 0 \tag{1}$$

This vector equation is subject to the incompressibility constraint condition given

below:

$$\nabla \cdot \mathbf{u} = 0 \tag{2}$$

All the variables in Eqs. (1)–(2) have been nondimensionalized by dividing the length by L_{ref}, the velocity vector by u_{ref}, and the pressure by ρu_{ref}^2, where ρ is the fluid density. The Reynolds number $\mathrm{Re} = \rho u_{\text{ref}} L_{\text{ref}} / \mu$ comes out as a direct result of normalization of dependent as well as independent variables.

For the elliptic differential equations to be well posed, Eqs. (1)–(2) must be subject to the following essential boundary condition at $\partial\Omega = \Gamma$:

$$\mathbf{u} = \mathbf{g} \tag{3}$$

where

$$\int_\Gamma \mathbf{n} \cdot \mathbf{g} \, d\Gamma = 0 \tag{4}$$

In Eq. (4), $\mathbf{n}$ denotes the unit outward normal to Γ. Under the circumstances, the following two equations on $\Gamma$are legitimate for the normal velocity g_n and tangential velocity g_r, respectively:

$$\mathbf{u} \cdot \mathbf{n} = g_n \qquad \text{on } \Gamma_n \tag{5}$$

and

$$\mathbf{n} \times \mathbf{u} \times \mathbf{n} = \mathbf{g}_r \qquad \text{on } \Gamma_r \tag{6}$$

It is important to note here that no boundary condition is permitted for the pressure on the boundary Γ when $\mathbf{g} = \mathbf{0}$ [2].

3. MIXED FINITE-ELEMENT FORMULATION

The solution to Eqs. (1)–(2) can be obtained using coupled formulation. Within this analysis framework, primitive variables $\mathbf{u}$ and p are solved directly from Eqs. (1)–(2), and we refer to this as the mixed formulation. Denote by $\mathcal{L}_0^2(\Omega)$ the constrained space for the pressure, which consists of square integrable functions having zero mean over Ω. In addition, we introduce the Sobolev space $\mathcal{H}_0^1(\Omega)$, which consists of one square integrable derivative over Ω and vanishes on the boundary Γ, for the vector-valued functions. Given the above two functional spaces, we seek $\mathbf{u} \in \mathcal{H}_0^1(\Omega)$ and $p \in \mathcal{L}_0^2(\Omega)$ from the following weak statement:

$$\begin{aligned} \int_\Omega (\mathbf{u} \cdot \nabla)\mathbf{u} \cdot \mathbf{w} \, d\Omega + \frac{1}{\mathrm{Re}} \int_\Omega \nabla \mathbf{u} : \nabla \mathbf{w} \, d\Omega - \int_\Omega p \nabla \cdot \mathbf{w} \, d\Omega \\ = \int_{\Gamma/\Gamma_n} r\mathbf{w} \cdot \mathbf{n} \, d\Gamma + \int_{\Gamma/\Gamma_r} \mathbf{s} \cdot \mathbf{w} \times \mathbf{n} \, d\Gamma \end{aligned} \tag{7}$$

$$\int_\Omega (\nabla \cdot \mathbf{u}) q \, d\Omega = 0 \tag{8}$$

where

$$-p + \frac{1}{\mathrm{Re}}\,\mathbf{n}\cdot\nabla\mathbf{u}\cdot\mathbf{n} = r \qquad \text{on } \frac{\Gamma}{\Gamma_n} \tag{9}$$

$$\frac{1}{\mathrm{Re}}\,\mathbf{n}\cdot\nabla\mathbf{u}\times\mathbf{n} = \mathbf{s} \qquad \text{on } \frac{\Gamma}{\Gamma_r} \tag{10}$$

In the above, $\mathbf{w}\,(\equiv N^i + B^i) \in \mathcal{H}_0^1(\Omega) \times \mathcal{H}_0^1(\Omega)$ and $q \in \mathcal{L}_0^2(\Omega)$ are the test functions for the vector and scalar quantities, respectively. We denote here two segments of the boundary Γ as Γ_n and Γ_r.The complement of Γ_i in Γ [or Γ/Γ_i $(i = n, r)$] is that if $\} \in \Gamma/\Gamma_i$, then $\} \in \Gamma$ but $\} \notin \Gamma_i$.

The guiding principle in the choice of finite-element basis functions is to avoid node-to-node pressure oscillations. One way of achieving this goal is to employ biquadratic polynomials, N_i, to approximate $\mathbf{u}$ by $\mathbf{u}^h = \sum u_i^h N_i^h$ and bilinear polynomials, M_i, to approximate p by $p^h = \sum p_i^h M_i^h$. This variable setting is endowed with the Ladyzhenskaya-Babuška-Brezzi (LBB) or inf-sup condition [4, 5] and is closely tied to storing the pressure and velocity unknowns in staggered meshes.

The assembled matrix equations for a problem having n^e elements take the form $\boldsymbol{A}\mathbf{q} = \mathbf{b}$ for the solution vector

$$\mathbf{q} = \begin{pmatrix} u_j \\ v_j \\ p_j \end{pmatrix} \tag{11}$$

The matrix $\boldsymbol{A}$ is expressed as

$$\begin{aligned} \boldsymbol{A} = [a_{ij}] = \sum_1^{n^e} \int_{\Omega^h} & \begin{pmatrix} C^{ij} & 0 & -M^j \dfrac{\partial N^i}{\partial x_1} + B^i \dfrac{\partial M^i}{\partial x_1} \\ 0 & C^{ij} & -M^j \dfrac{\partial N^i}{\partial x_2} + B^i \dfrac{\partial M^i}{\partial x_2} \\ M^i \dfrac{\partial N^j}{\partial x_1} & M^i \dfrac{\partial N^j}{\partial x_2} & 0 \end{pmatrix} d\Omega^h \\ + \int_{\Gamma^h} & \begin{pmatrix} -\dfrac{1}{\mathrm{Re}}\left(N^i \dfrac{\partial N^j}{\partial x_k}\right)\cdot n_k & 0 & 0 \\ 0 & -\dfrac{1}{\mathrm{Re}}\left(N^i \dfrac{\partial N^j}{\partial x_k}\right)\cdot n_k & 0 \\ 0 & 0 & 0 \end{pmatrix} d\Gamma^h \end{aligned} \tag{12}$$

where

$$C^{ij} = (N^i + B^i) N^j \tilde{V}_k^j \frac{\partial N^j}{\partial x_k} + \frac{1}{\mathrm{Re}} \frac{\partial N^i}{\partial x_k} \frac{\partial N^j}{\partial x_k} - \frac{1}{\mathrm{Re}} B^i \frac{\partial^2 N^j}{\partial x_k \partial x_k} \tag{13}$$

In practice, it is customary to set the value of $\tilde{V}_k^j$ as a constant when evaluating the finite-element matrices. It is noted that the line integral shown in Eq. (12) is attributed to the prescribed essential boundary conditions. As to boundaries where

natural boundary conditions are imposed, they are shown in the **b** vector,

$$\mathbf{b} = \int_{\Gamma^h} \begin{pmatrix} -N^i p_i n_1 \\ -N^i p_i n_2 \\ 0 \end{pmatrix} d\Gamma^h \tag{14}$$

where the vector (n_1, n_2) is locally orthogonal to the boundary, at which pressure values are imposed.

In the numerical simulation of high Reynolds number flows, selection of the test space **w** is vital to suppressing velocity oscillations [3]. Within the Petrov–Galerkin finite-element framework, we have enhanced the discrete system through modification of the Galerkin method by adding a biased polynomial B^i shown in Eq. (13),

$$B^i = \tau N^j \tilde{V}_k^j \frac{\partial N^i}{\partial x_k} \tag{15}$$

to the basis function, N^j. The direct result is that field variables on the upwind side are favorably considered [3]. With a view to constructing a computationally excellent Petrov–Galerkin model, it is desired that in Eq. (15) the free parameter τ, which determines the degree of upwinding needed to suppress oscillatory velocities, can be derived theoretically. Take the following linear convection-diffusion equation as an example,

$$u \frac{\partial \phi}{\partial x} - \frac{1}{\mathrm{Re}} \frac{\partial^2 \phi}{\partial x^2} = 0 \tag{16}$$

we make use of its analytical solution,

$$\phi_{\text{exact}} = C_1 + C_2 \exp(u \,\mathrm{Re}\, x) \tag{17}$$

in the derivation of Petrov–Galerkin finite-element model in a domain of one dimension. In the above, C_1 and C_2 are two constants. Assuming that $\phi = \sum_{i=1}^{3} N_i \phi_i$ and $W_j = N_j + \tau u(\partial N_j / \partial x)$, we substitute them into the weak representation of Eq. (16). After some algebra, the discrete equations at two end nodes and one center node can be derived. By substituting the exact expressions of $\phi_i, \phi_{i\pm1}, \phi_{i\pm2}$, obtained from Eq. (17), into these discrete equations, we can derive τ analytically at the center and end nodes,

$$\tau = \frac{\delta u H}{2|u|^2} \tag{18}$$

where H represents the grid size. Considering nodes of different classification, δ is chosen as follows to obtain their exact expressions on quadratic elements:

$$\delta = \begin{cases} \dfrac{2 - \cosh(\gamma) - (4/\gamma)\tanh(\gamma/2) + (1/\gamma)\sinh(\gamma)}{4\tanh(\gamma/2) - \sinh(\gamma) - (6/\gamma)\sinh(\gamma)\tanh(\gamma/2)} & \text{at end nodes} \\ \dfrac{1}{2}\coth\left(\dfrac{\gamma}{2}\right) - \dfrac{1}{\gamma} & \text{at center nodes} \end{cases} \tag{19}$$

where

$$\gamma = \frac{uH\mathrm{Re}}{2}$$

For the sake of completeness, we plot δ against Peclet number γ in Figure 1.

The extension of the above finite-element formulation to multidimensional analysis is, however, obtained at the cost of accuracy. The reason is that use of the conventional Petrov–Galerkin model has a tendency to add false diffusion errors to regions normal to the streamline as the angle between the grid line and the flow direction is considerable. To improve upon this situation, the chosen weighting functions should accommodate a streamline operator so as to provide a natural mechanism for adding artificial diffusivity in the primary flow direction only. In biquadratic elements, the following upwinding coefficients are assigned at the center

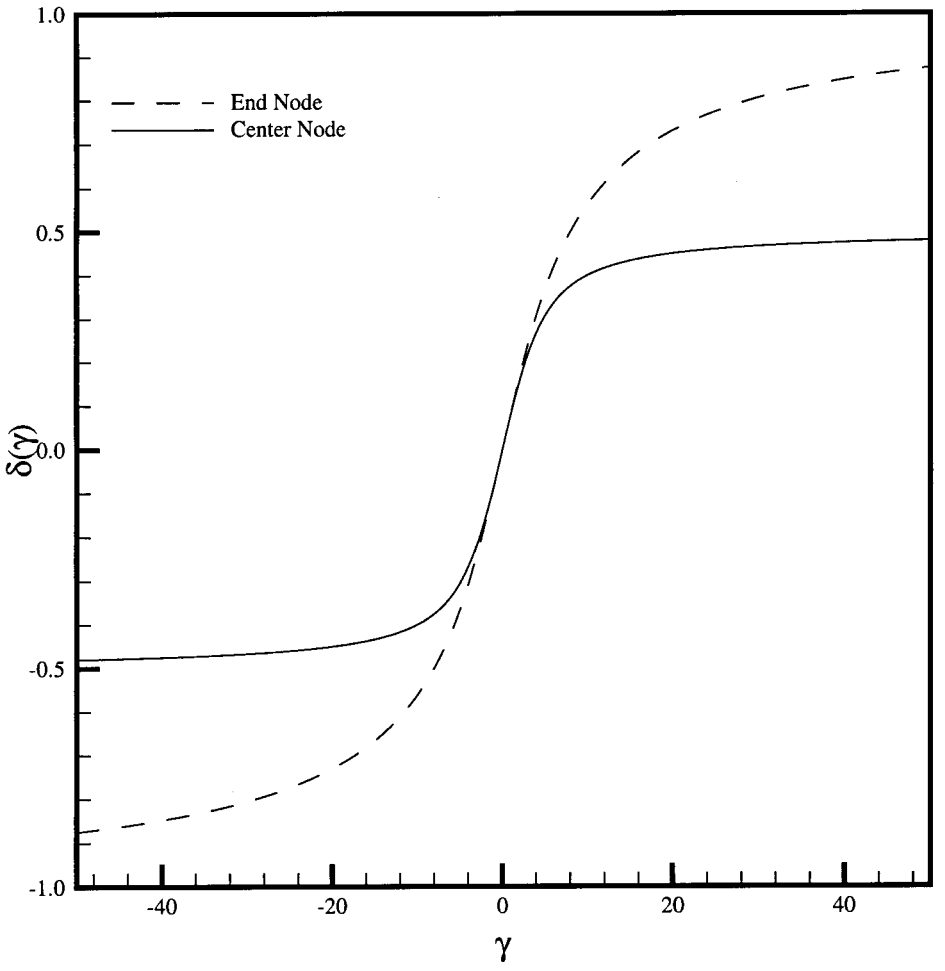

Figure 1. Upwinding coefficient τ, defined in Eq. (19), against Peclet numbers γ in a biquadratic element.

and end nodes to stabilize the discrete system [6]:

$$\tau = \frac{\sum_{i=1}^{n} \delta(\gamma_{Y_i}) V_{Y_i} h}{2(u^2 + v^2)^2} \tag{20}$$

In the above, δ is obtained on the one-dimensional basis

$$\delta(\gamma) = \begin{cases} \dfrac{2 - \cosh(\gamma) - (4/\gamma)\tanh(\gamma/2) + (1/\gamma)\sinh(\gamma)}{4\tanh(\gamma/2) - \sinh(\gamma) - (6/\gamma)\sinh(\gamma)\tanh(\gamma/2)} & \text{at end nodes} \\ \dfrac{1}{2}\coth\left(\dfrac{\gamma}{2}\right) - \dfrac{1}{\gamma} & \text{at center nodes} \end{cases} \tag{21}$$

where $\gamma_{Y_i} = V_{Y_i} \mathrm{Re} h/2$, and Y_i denotes the local coordinates ξ and η.

4. THEORETICAL ANALYSIS

Like the work of Pepper and Baker [13], we can also rewrite the discretized finite-element equation to a form akin to that of the finite-difference equations. Both continuity and linearized momentum equations have been investigated in this regard.

Continuity Equation

To analyze the discrete problem for Eqs. (7)–(10), we carry out expansion of $\mathbf{u}$ and p using basis functions and substitute them into Eqs. (7)–(8). This is followed by substitution of test functions into the weak statement to obtain the following discrete conservation equation for the mass at the nodal point (i, j):

$$\begin{aligned} &\frac{1}{9h}(-u_{i-2,j-1} - 4u_{i-1,j-1} + 4u_{i+1,j-1} + u_{i+2,j-1} - u_{i-2,j} - 4u_{i-1,j} + 4u_{i+1,j} \\ &\quad + u_{i+2,j} - u_{i-2,j+1} - 4u_{i-1,j+1} + 4u_{i+1,j+1} + u_{i+2,j+1}) \\ &\quad + \frac{1}{9h}(-v_{i-1,j-2} - 4v_{i-1,j-1} + 4v_{i-1,j+1} + v_{i-1,j+2} - v_{i,j-2} - 4v_{i,j-1} + 4v_{i,j+1} \\ &\quad + v_{i,j+2} - v_{i+1,j-2} - 4v_{i+1,j-1} + 4v_{i+1,j+1} + v_{i+1,j+2}) = 0 \end{aligned} \tag{22}$$

To better elucidate on how well the divergence-free condition is satisfied, complementary modified equation analysis was therefore undertaken. By conducting Taylor series expansion on the terms shown in the discrete continuity equation (22), the following modified equation is derived:

$$\begin{aligned} u_x + v_y = &-\left(\frac{h^2}{3}u_{xxx} + \frac{h^2}{3}u_{xyy} + \frac{h^4}{20}u_{xxxxx} + \frac{h^4}{9}u_{xxxyy} + \frac{h^4}{36}u_{xyyyy}\right) \\ &-\left(\frac{h^2}{3}v_{xxy} + \frac{h^2}{3}v_{yyy} + \frac{h^4}{36}v_{xxxxy} + \frac{h^4}{9}v_{xxyyy} + \frac{h^4}{20}v_{yyyyy}\right) + \mathcal{O}(h^6) \end{aligned} \tag{23}$$

Clearly seen from the above equation is that Eq. (2) is approached as the grid size h continues to decrease. This provides justification for the validity of the mixed finite-element formulation for incompressible fluid flows.

Momentum Equations

In the derivation of discrete equations of motion in biquadratic elements, we must divide the elements into four types to complete the formulation. According to the finite elements shown schematically in Figure 2, the discrete representation of the momentum equations can be obtained. Due to space limitation, we omit the detailed derivation of these equations but summarize them in Tables 1–4. To explore in more detail the streamline-upwinding Petrov–Galerkin finite-element model, we now turn our attention to modified equation analysis of the linearized momentum equations, which involve constant velocities a and b along the x and y direction, respectively. A detailed derivation of these equations is mathematically lengthy and will not be presented here for the sake of brevity. We simply summarize them below for the reader's reference.

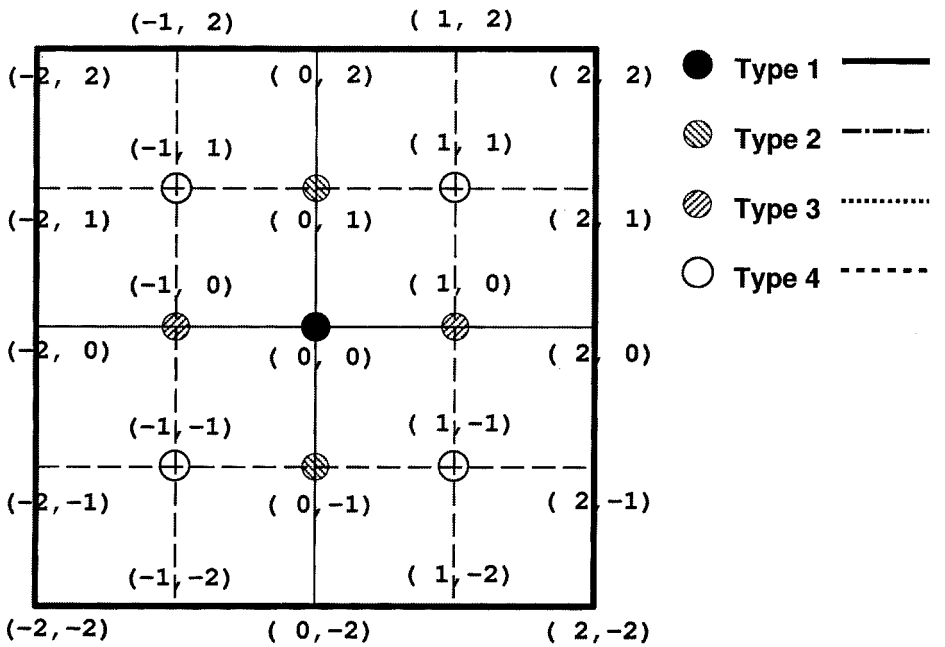

Figure 2. Notations used in the classification of elements for the derivation of discrete momentum equations.

Table 1. Discretized momentum equations for the type 1 element:

$$\sum_{i=-2}^{2}\sum_{j=-2}^{2} a_{ij}u_{ij} + \sum_{i=-2}^{2}\sum_{j=-2}^{2} b_{ij}p_{ij} = 0$$

Element type node number	Type 1		
Reference node	a_{ij} (taking (0, 0) as an example)	b_{ij} (x momentum)	b_{ij} (y momentum)
Node $(i-2, j-2)$	$-\frac{1}{90}\frac{b^2h\,\mathrm{Re}\,\tau+h^2\,\mathrm{Re}\,a+5h\,\mathrm{Re}\,b\tau a+bh^2\,\mathrm{Re}-11\tau b-11\tau a+h\,\mathrm{Re}\,\tau a^2+2h}{\mathrm{Re}\,h^3}$	$-\frac{1}{36}\frac{\tau b}{h^2}$	$-\frac{1}{36}\frac{\tau a}{h^2}$
Node $(i-1, j-2)$	$\frac{1}{45}\frac{b^2h\,\mathrm{Re}\,\tau+2h^2\,\mathrm{Re}\,a+10h\,\mathrm{Re}\,b\tau a+bh^2\,\mathrm{Re}-11\tau b-16\tau a+4h\,\mathrm{Re}\,\tau a^2+5h}{\mathrm{Re}\,h^3}$		
Node $(i, j-2)$	$\frac{1}{45}\frac{-19\tau b-7h\,\mathrm{Re}\,\tau a^2+4bh^2\,\mathrm{Re}-3h+4b^2\,\mathrm{Re}\,\tau}{\mathrm{Re}\,h^3}$		$-\frac{1}{9}\frac{3\tau b+h}{h^2}$
Node $(i+1, j-2)$	$-\frac{1}{45}\frac{-b^2h\,\mathrm{Re}\,\tau+2h^2\,\mathrm{Re}\,a+10h\,\mathrm{Re}\,b\tau a-bh^2\,\mathrm{Re}+11\tau b-16\tau a-4h\,\mathrm{Re}\,\tau a^2-5h}{\mathrm{Re}\,h^3}$		
Node $(i+2, j-2)$	$\frac{1}{90}\frac{-b^2h\,\mathrm{Re}\,\tau+h^2\,\mathrm{Re}\,a+5h\,\mathrm{Re}\,b\tau a-bh^2\,\mathrm{Re}+11\tau b-11\tau a-h\,\mathrm{Re}\,\tau a^2-2h}{\mathrm{Re}\,h^3}$	$\frac{1}{36}\frac{\tau b}{h^2}$	$\frac{1}{36}\frac{\tau a}{h^2}$
Node $(i-2, j-1)$	$\frac{1}{45}\frac{4b^2h\,\mathrm{Re}\,\tau+h^2\,\mathrm{Re}\,a+10h\,\mathrm{Re}\,b\tau a+2bh^2\,\mathrm{Re}-16\tau b-11\tau a+h\,\mathrm{Re}\,\tau a^2+5h}{\mathrm{Re}\,h^3}$		
Node $(i-1, j-1)$	$-\frac{4}{45}\frac{2b^2h\,\mathrm{Re}\,\tau+h^2\,\mathrm{Re}\,a+10h\,\mathrm{Re}\,b\tau a+bh^2\,\mathrm{Re}-8\tau b-8\tau a+2h\,\mathrm{Re}\,\tau a^2+4h}{\mathrm{Re}\,h^3}$		
Node $(i, j-1)$	$-\frac{2}{45}\frac{-14\tau b-7h\,\mathrm{Re}\,\tau a^2+8bh^2\,\mathrm{Re}+9h+16b^2h\,\mathrm{Re}\,\tau}{\mathrm{Re}\,h^3}$		
Node $(i+1, j-1)$	$\frac{4}{45}\frac{-2b^2h\,\mathrm{Re}\,\tau+h^2\,\mathrm{Re}\,a+10h\,\mathrm{Re}\,b\tau a-bh^2\,\mathrm{Re}+8\tau b-8\tau a-2h\,\mathrm{Re}\,\tau a^2-4h}{\mathrm{Re}\,h^3}$		
Node $(i+2, j-1)$	$-\frac{1}{45}\frac{-4b^2h\,\mathrm{Re}\,\tau+h^2\,\mathrm{Re}\,a+10h\,\mathrm{Re}\,b\tau a-2bh^2\,\mathrm{Re}+16\tau b-11\tau a-h\,\mathrm{Re}\,\tau a^2-5h}{\mathrm{Re}\,h^3}$		
Node $(i-2, j)$	$\frac{1}{45}\frac{-19\tau a+4h^2\,\mathrm{Re}\,a+4h\,\mathrm{Re}\,\tau a^2-7b^2h\,\mathrm{Re}\,\tau-3h}{\mathrm{Re}\,h^3}$	$-\frac{1}{9}\frac{h+3\tau a}{h^2}$	
Node $(i-1, j)$	$-\frac{2}{45}\frac{-14\tau a+8h^2\,\mathrm{Re}\,a-7b^2h\,\mathrm{Re}\,\tau+16h\,\mathrm{Re}\,\tau a^2+9h}{\mathrm{Re}\,h^3}$		
Node (i, j)	$\frac{56}{45}\frac{\mathrm{Re}\,\tau a^2+2+b^2\,\mathrm{Re}\,\tau}{h^2\,\mathrm{Re}}$	$\frac{2}{3}\frac{\tau a}{h^2}$	$\frac{2}{3}\frac{\tau b}{h^2}$
Node $(i+1, j)$	$\frac{2}{45}\frac{-14\tau a+8h^2\,\mathrm{Re}\,a+7b^2h\,\mathrm{Re}\,\tau-16h\,\mathrm{Re}\,Ta^2-9h}{\mathrm{Re}\,h^3}$		
Node $(i+2, j)$	$-\frac{1}{45}\frac{-19\tau a+4h^2\,\mathrm{Re}\,a-4h\,\mathrm{Re}\,\tau a^2+7b^2h\,\mathrm{Re}\,\tau+3h}{\mathrm{Re}\,h^3}$	$-\frac{1}{9}\frac{-h+3\tau a}{h^2}$	

Table 1. *continued*

Element type node number	Type 1		
Reference node	a_{ij} (Taking (0, 0) as an example	b_{ij} (x momentum)	b_{ij} (y momentum)
Node $(i-2, j+1)$	$\frac{1}{45}\frac{4b^2h\,\mathrm{Re}\,\tau+h^2\,\mathrm{Re}\,a-10h\,\mathrm{Re}\,b\tau a-2bh^2\,\mathrm{Re}+16\tau b-11\tau a+h\,\mathrm{Re}\,\tau a^2+5h}{\mathrm{Re}\,h^3}$		
Node $(i-1, j+1)$	$-\frac{4}{45}\frac{2b^2h\,\mathrm{Re}\,\tau+h^2\,\mathrm{Re}\,a-10h\,\mathrm{Re}\,b\tau a-bh^2\,\mathrm{Re}+8\tau b-8\tau a+2h\,\mathrm{Re}\,\tau a^2+4h}{\mathrm{Re}\,h^3}$		
Node $(i, j+1)$	$\frac{2}{45}\frac{-14\tau b+7h\,\mathrm{Re}\,\tau a^2+8bh^2\,\mathrm{Re}-9h-16b^2h\,\mathrm{Re}\,\tau}{\mathrm{Re}\,h^3}$		
Node $(i+1, j+1)$	$\frac{4}{45}\frac{-2b^2h\,\mathrm{Re}\,\tau+h^2+h^2\,\mathrm{Re}\,a-10h\,\mathrm{Re}\,b\tau a+bh^2\,\mathrm{Re}-8\tau b-8\tau a-2h\,\mathrm{Re}\,\tau a^2-4h}{\mathrm{Re}\,h^3}$		
Node $(i+2, j+1)$	$-\frac{1}{45}\frac{-4b^2h\,\mathrm{Re}\,\tau+h^2\,\mathrm{Re}\,a-10h\,\mathrm{Re}\,b\tau a+2bh^2\,\mathrm{Re}-16\tau b-11\tau a-h\,\mathrm{Re}\,\tau a^2-5h}{\mathrm{Re}\,h^3}$		
Node $(i-2, j+2)$	$-\frac{1}{90}\frac{b^2h\,\mathrm{Re}\,\tau+h^2\,\mathrm{Re}\,a-5h\,\mathrm{Re}\,b\tau a-bh^2\,\mathrm{Re}+11\tau b-11\tau a+h\,\mathrm{Re}\,\tau a^2+2h}{\mathrm{Re}\,h^3}$	$\frac{1}{36}\frac{\tau b}{h^2}$	$\frac{1}{36}\frac{\tau a}{h^2}$
Node $(i-1, j+2)$	$\frac{1}{45}\frac{b^2h\,\mathrm{Re}\,\tau+2h^2\,\mathrm{Re}\,a-10h\,\mathrm{Re}\,b\tau a-bh^2\,\mathrm{Re}+11\tau b-16\tau a+4h\,\mathrm{Re}\,\tau a^2+5h}{\mathrm{Re}\,h^3}$		
Node $(i, j+2)$	$-\frac{1}{45}\frac{-19\tau b+7h\,\mathrm{Re}\,\tau a^2+4bh^2\,\mathrm{Re}+3h-4b^2h\mathrm{Re}\,\tau}{\mathrm{Re}\,h^3}$		$\frac{1}{9}\frac{h-3\tau b}{h^2}$
Node $(i+1, j+2)$	$-\frac{1}{45}\frac{-b^2h\,\mathrm{Re}\,\tau+2h^2\,\mathrm{Re}\,a-10h\,\mathrm{Re}\,b\tau a+bh^2\,\mathrm{Re}-11\tau b-16\tau a-4h\,\mathrm{Re}\,\tau a^2-5h}{\mathrm{Re}\,h^3}$		
Node $(i+2, j+2)$	$\frac{1}{90}\frac{bh^2\,\mathrm{Re}+h^2\,\mathrm{Re}\,a-5h\,\mathrm{Re}\,b\tau a-b^2h\,\mathrm{Re}\,\tau-11\tau b-11\tau a-h\,\mathrm{Re}\,\tau a^2-2h}{\mathrm{Re}\,h^3}$	$-\frac{1}{36}\frac{\tau b}{h^2}$	$-\frac{1}{36}\frac{\tau a}{h^2}$

Table 2. Discretized momentum equations for the type 2 element:

$$\sum_{i=-2}^{2}\sum_{j=-2}^{2} a_{ij}u_{ij} + \sum_{i=-2}^{2}\sum_{j=-2}^{2} b_{ij}p_{ij} = 0$$

Element type node number	Type 2		
Reference node	a_{ij} (taking (0, −1) as an example)	b_{ij} (x momentum)	b_{ij} (y momentum)
Node $(i-2, j-2)$	$\frac{1}{45}\frac{4b^2h\,\mathrm{Re}\,\tau+h^2\,\mathrm{Re}\,a+10h\,\mathrm{Re}\,b\tau a+2bh^2\,\mathrm{Re}-10\tau b+4\tau a+h\,\mathrm{Re}\,\tau a^2+5h}{\mathrm{Re}\,h^3}$	$-\frac{1}{9}\frac{h+3\tau a+\tau b}{h^2}$	$-\frac{1}{9}\frac{\tau a}{h^2}$
Node $(i-1, j-2)$	$-\frac{4}{45}\frac{2b^2h\,\mathrm{Re}\,\tau+h^2\,\mathrm{Re}\,a+10h\,\mathrm{Re}\,b\tau a+bh^2\,\mathrm{Re}-5\tau b+7\tau a+2h\,\mathrm{Re}\,\tau a^2+4h}{\mathrm{Re}\,h^3}$		
Node $(i, j-2)$	$-\frac{2}{45}\frac{10\tau b-7h\,\mathrm{Re}\,\tau a^2+8bh^2\,\mathrm{Re}+9h+16Ay^2h\,\mathrm{Re}\,\tau}{\mathrm{Re}\,h^3}$	$\frac{2}{3}\frac{\tau a}{h^2}$	$-\frac{4}{9}\frac{1}{h}$
Node $(i+1, j-2)$	$\frac{4}{45}\frac{-2b^2h\,\mathrm{Re}\,\tau+h^2\,\mathrm{Re}\,a+10h\,\mathrm{Re}\,b\tau a-bh^2\,\mathrm{Re}+5\tau b+7\tau a-2h\,\mathrm{Re}\,\tau a^2-4h}{\mathrm{Re}\,h^3}$		
Node $(i+2, j-2)$	$-\frac{1}{45}\frac{-4b^2h\,\mathrm{Re}\,\tau+h^2\,\mathrm{Re}\,a+10h\,\mathrm{Re}\,b\tau a-2bh^2\,\mathrm{Re}+10\tau b+4\tau a-h\,\mathrm{Re}\,\tau a^2-5h}{\mathrm{Re}\,h^3}$	$-\frac{1}{9}\frac{-h+3\tau a-\tau b}{h^2}$	$\frac{1}{9}\frac{\tau a}{h^2}$
Node $(i-2, j-1)$	$\frac{4}{45}\frac{2h\,\mathrm{Re}\,\tau a^2+2h^2\,\mathrm{Re}\,a-17\tau a-2b^2h\,\mathrm{Re}\,\tau}{\mathrm{Re}\,h^3}$		
Node $(i-1, j-1)$	$-\frac{16}{45}\frac{4h\,\mathrm{Re}\,\tau a^2+2h^2\,\mathrm{Re}\,a-11\tau a-b^2h\,\mathrm{Re}\,\tau+3h}{\mathrm{Re}\,h^3}$		
Node $(i, j-1)$	$\frac{16}{45}\frac{7\,\mathrm{Re}\,\tau a^2+11+4b^2\,\mathrm{Re}\,\tau}{h^2\,\mathrm{Re}}$		
Node $(i+1, j-1)$	$\frac{16}{45}\frac{-4h\,\mathrm{Re}\,\tau a^2+2h^2\,\mathrm{Re}\,a-11\tau a+b^2h\,\mathrm{Re}\,\tau-3h}{\mathrm{Re}\,h^3}$		
Node $(i+2, j-1)$	$-\frac{4}{45}\frac{-2h\,\mathrm{Re}\,\tau a^2+2h^2\,\mathrm{Re}\,a-17\tau a+2b^2h\,\mathrm{Re}\,\tau}{\mathrm{Re}\,h^3}$		
Node $(i-2, j)$	$\frac{1}{45}\frac{4b^2h\,\mathrm{Re}\,\tau+h^2\,\mathrm{Re}\,a-10h\,\mathrm{Re}\,b\tau a-2bh^2\,\mathrm{Re}+10\tau b+4\tau a+h\,\mathrm{Re}\,\tau a^2+5h}{\mathrm{Re}\,h^3}$	$-\frac{1}{9}\frac{h+3\tau a-\tau b}{h^2}$	$\frac{1}{9}\frac{\tau a}{h^2}$
Node $(i-1, j)$	$-\frac{4}{45}\frac{2b^2h\,\mathrm{Re}\,\tau+h^2\,\mathrm{Re}\,a-10h\,\mathrm{Re}\,b\tau a-bh^2\,\mathrm{Re}+5\tau b+7\tau a+2h\,\mathrm{Re}\,\tau a^2+4h}{\mathrm{Re}\,h^3}$		
Node (i, j)	$\frac{2}{45}\frac{10\tau b+7h\,\mathrm{Re}\,\tau a^2+8bh^2\,\mathrm{Re}-9h-16b^2h\mathrm{Re}\,\tau}{\mathrm{Re}\,h^3}$	$\frac{2}{3}\frac{\tau a}{h^2}$	$\frac{4}{9}\frac{1}{h}$
Node $(i+1, j)$	$\frac{4}{45}\frac{-2b^2h\,\mathrm{Re}\,\tau+h^2\,\mathrm{Re}\,a-10h\,\mathrm{Re}\,b\tau a+bh^2\,\mathrm{Re}-5\tau b+7\tau a-2h\,\mathrm{Re}\,\tau a^2-4h}{\mathrm{Re}\,h^3}$		
Node $(i+2, j)$	$-\frac{1}{45}\frac{-4b^2h\,\mathrm{Re}\,\tau+h^2\,\mathrm{Re}\,a-10h\,\mathrm{Re}\,b\tau a+2bh^2\,\mathrm{Re}-10\tau b+4\tau a-h\,\mathrm{Re}\,\tau a^2-5h}{\mathrm{Re}\,h^3}$	$-\frac{1}{9}\frac{-h+3\tau a+\tau b}{h^2}$	$-\frac{1}{9}\frac{\tau a}{h^2}$

Table 3. Discretized momentum equations for the type 3 element:

$$\sum_{i=-2}^{2}\sum_{j=-2}^{2} a_{ij}u_{ij} + \sum_{i=-2}^{2}\sum_{j=-2}^{2} b_{ij}p_{ij} = 0$$

Element type node number	Type 3		
Reference node	a_{ij} (taking $(-1, 0)$ as an example)	b_{ij} (x momentum)	b_{ij} (y momentum)
Node $(i-2, j-2)$	$\frac{1}{45}\frac{4h\,\mathrm{Re}\,\tau a^2+2h^2\,\mathrm{Re}\,a+10h\,\mathrm{Re}\,b\tau a+5h+4\tau b-10\tau a+bh^2\,\mathrm{Re}+b^2h\,\mathrm{Re}\tau}{\mathrm{Re}\,h^3}$	$-\frac{1}{9}\frac{\tau b}{h^2}$	$-\frac{1}{9}\frac{3\tau b+\tau a+h}{h^2}$
Node $(i-1, j-2)$	$\frac{4}{45}\frac{2b^2h\,\mathrm{Re}\,\tau-2h\,\mathrm{Re}\,\tau a^2+2bh^2\,\mathrm{Re}-17\tau b}{\mathrm{Re}\,h^3}$		
Node $(i, j-2)$	$-\frac{1}{45}\frac{-4h\,\mathrm{Re}\,\tau a^2+2h^2\,\mathrm{Re}\,a+10h\,\mathrm{Re}\,b\tau a-5h-4\tau b-10\tau a-bh^2\,\mathrm{Re}-b^2h\,\mathrm{Re}\,\tau}{\mathrm{Re}\,h^3}$	$\frac{1}{9}\frac{\tau b}{h^2}$	$-\frac{1}{9}\frac{3\tau b-\tau a+h}{h^2}$
Node $(i-2, j-1)$	$-\frac{4}{45}\frac{2h\,\mathrm{Re}\,\tau a^2+h^2\,\mathrm{Re}\,a+10h\,\mathrm{Re}\,b\tau a+4h+7\tau b-5\tau a+bh^2\,\mathrm{Re}+2b^2h\,\mathrm{Re}\,\tau}{\mathrm{Re}\,h^3}$		
Node $(i-1, j-1)$	$-\frac{16}{45}\frac{4b^2h\,\mathrm{Re}\,\tau-h\,\mathrm{Re}\tau a^2+2bh^2\,\mathrm{Re}-11\tau b+3h}{\mathrm{Re}\,h^3}$		
Node $(i, j-1)$	$\frac{4}{45}\frac{-2h\,\mathrm{Re}\,\tau a^2+h^2\,\mathrm{Re}\,a+10h\,\mathrm{Re}\,b\tau a-4h-7\tau b-5\tau a-bh^2\,\mathrm{Re}-2b^2h\,\mathrm{Re}\tau}{\mathrm{Re}\,h^3}$		
Node $(i-2, j)$	$-\frac{2}{45}\frac{10\tau a+8h^2\,\mathrm{Re}\,a+16h\,\mathrm{Re}\,\tau a^2-7b^2h\,\mathrm{Re}\,\tau+9h}{\mathrm{Re}\,h^3}$	$-\frac{4}{9}\frac{1}{h}$	$\frac{2}{3}\frac{\tau b}{h^2}$
Node $(i-1, j)$	$\frac{16}{45}\frac{11+7b^2\,\mathrm{Re}\,\tau+4\,\mathrm{Re}\,\tau a^2}{h^2\,\mathrm{Re}}$		
Node (i, j)	$\frac{2}{45}\frac{10\tau a+8h^2\,\mathrm{Re}\,a-16h\,\mathrm{Re}\,\tau a^2+7b^2h\,\mathrm{Re}\,\tau-9h}{\mathrm{Re}\,h^3}$	$\frac{4}{9}\frac{1}{h}$	$\frac{2}{3}\frac{\tau b}{h^2}$
Node $(i-2, j+1)$	$-\frac{4}{45}\frac{2h\,\mathrm{Re}\,\tau a^2+h^2\,\mathrm{Re}\,a-10h\,\mathrm{Re}\,b\tau a+4h-7\tau b-5\tau a-bh^2\,\mathrm{Re}+2b^2h\,\mathrm{Re}\,\tau}{\mathrm{Re}\,h^3}$		
Node $(i-1, j+1)$	$\frac{16}{45}\frac{-4b^2h\,\mathrm{Re}\,\tau+h\,\mathrm{Re}\,\tau a^2+2bh^2\,\mathrm{Re}-11\tau b-3h}{\mathrm{Re}\,h^3}$		
Node $(i, j+1)$	$\frac{4}{45}\frac{-2h\,\mathrm{Re}\,\tau a^2+h^2\,\mathrm{Re}\,a-10h\,\mathrm{Re}\,b\tau a-4h+7\tau b-5\tau a+bh^2\,\mathrm{Re}-2b^2h\ \mathrm{Re}\,\tau}{\mathrm{Re}\,h^3}$		
Node $(i-2, j+2)$	$\frac{1}{45}\frac{-4\tau b+2h^2\,\mathrm{Re}\,a-10h\,\mathrm{Re}\,b\tau a-bh^2\,\mathrm{Re}+b^2h\,\mathrm{Re}\,\tau-10\tau a+4h\,\mathrm{Re}\,\tau a^2+5h}{\mathrm{Re}\,h^3}$	$\frac{1}{9}\frac{\tau b}{h^2}$	$\frac{1}{9}\frac{\tau a+h-3\tau b}{h^2}$
Node $(i-1, j+2)$	$-\frac{4}{45}\frac{-2b^2h\,\mathrm{Re}\tau+2h\,\mathrm{Re}\,\tau a^2+2bh^2\,\mathrm{Re}-17\tau b}{\mathrm{Re}\,h^3}$		
Node $(i, j+2)$	$-\frac{1}{45}\frac{4\tau b+2h^2\,\mathrm{Re}\,a-10h\,\mathrm{Re}\,b\tau a+bh^2\,\mathrm{Re}-b^2h\,\mathrm{Re}\,\tau a-10\tau a-4h\,\mathrm{Re}\,\tau a^2-5h}{\mathrm{Re}\,h^3}$	$-\frac{1}{9}\frac{\tau b}{h^2}$	$\frac{1}{9}\frac{-\tau a+h-3\tau b}{h^2}$

Table 4. Discretized momentum equations for the type 4 element:

$$\sum_{i=-2}^{2}\sum_{j=-2}^{2} a_{ij}u_{ij} + \sum_{i=-2}^{2}\sum_{j=-2}^{2} b_{ij}p_{ij} = 0$$

Element type node number	Type 4		
Reference node	a_{ij} (taking $(-1, -1)$ as an example)	b_{ij} (x momentum)	b_{ij} (y momentum)
Node $(i-2, j-2)$	$-\frac{4}{45}\frac{10h\,\mathrm{Re}\,b\tau a+10\tau a+2h\,\mathrm{Re}\,\tau a^2+h^2\,\mathrm{Re}\,a+10\tau b+2b^2h\,\mathrm{Re}\,\tau+bh^2\,\mathrm{Re}+4h}{\mathrm{Re}\,h^3}$	$-\frac{4}{9}\frac{h+\tau b}{h^2}$	$-\frac{4}{9}\frac{\tau a+h}{h^2}$
Node $(i-1, j-2)$	$-\frac{16}{45}\frac{4b^2h\,\mathrm{Re}\,\tau-h\,\mathrm{Re}\,\tau a^2+2bh^2\,\mathrm{Re}-5\tau b+3h}{\mathrm{Re}\,h^3}$		
Node $(i, j-2)$	$\frac{4}{45}\frac{10h\,\mathrm{Re}\,b\tau a+10\tau a-2h\,\mathrm{Re}\,\tau a^2+h^2\,\mathrm{Re}\,a-10\tau b-2b^2h\,\mathrm{Re}\tau-bh^2\,\mathrm{Re}-4h}{\mathrm{Re}\,h^3}$	$\frac{4}{9}\frac{h+\tau b}{h^2}$	$-\frac{4}{9}\frac{\tau a+h}{h^2}$
Node $(i-2, j-1)$	$-\frac{16}{45}\frac{4h\,\mathrm{Re}\,\tau a^2+3h+2h^2\,\mathrm{Re}\,a-5\tau a-b^2h\mathrm{Re}\,\tau}{\mathrm{Re}\,h^3}$		
Node $(i-1, j-1)$	$\frac{128}{45}\frac{\mathrm{Re}\tau a^2+2+b^2\,\mathrm{Re}\,\tau}{h^2\,\mathrm{Re}}$		
Node $(i, j-1)$	$\frac{16}{45}\frac{-4h\,\mathrm{Re}\,\tau a^2-3h+2h^2\,\mathrm{Re}\,a-5\tau a+b^2h\,\mathrm{Re}\,\tau}{\mathrm{Re}\,h^3}$		
Node $(i-2, j)$	$-\frac{4}{45}\frac{-10h\,\mathrm{Re}\,b\tau a+10\tau Ax+2h\,\mathrm{Re}\,\tau a^2+h^2\,\mathrm{Re}\,Ax-10\tau b^2h\,\mathrm{Re}\,\tau-bh^2\,\mathrm{Re}+4h}{\mathrm{Re}\,h^3}$	$\frac{4}{9}\frac{-h+\tau b}{h^2}$	$\frac{4}{9}\frac{\tau a+h}{h^2}$
Node $(i-1, j)$	$\frac{16}{45}\frac{-4b^2h\,\mathrm{Re}\,\tau+h\,\mathrm{Re}\,\tau a^2+2bh^2\,\mathrm{Re}-5\tau b-3h}{\mathrm{Re}\,h^3}$		
Node (i, j)	$\frac{4}{45}\frac{-10h\,\mathrm{Re}\,b\tau a+10\tau a-2h\,\mathrm{Re}\,\tau a^2+h^2\,\mathrm{Re}\,a+10\tau b-2b^2h\,\mathrm{Re}\,\tau+bh^2\,\mathrm{Re}-4h}{\mathrm{Re}\,h^3}$	$-\frac{4}{9}\frac{-h+\tau b}{h^2}$	$\frac{4}{9}\frac{-\tau a+h}{h^2}$

Type 1:

$$
\begin{aligned}
&au_x + bu_y + p_x - \frac{1}{\mathrm{Re}}(u_{xx} + u_{yy}) = a^2\tau u_{xx} + 2ab\tau u_{xy} + b^2\tau u_{yy} \\
&\quad + \frac{1}{3}\,\frac{a(-9\tau + h^2\,\mathrm{Re})}{\mathrm{Re}}u_{xxx} + \frac{1}{5}\,\frac{b(-5\tau + h^2\,\mathrm{Re})}{\mathrm{Re}}u_{xxy} \\
&\quad + \frac{1}{5}\,\frac{a(-5\tau + h^2\,\mathrm{Re})}{\mathrm{Re}}u_{xyy} + \frac{1}{3}\,\frac{b(-9\tau + h^2\,\mathrm{Re})}{\mathrm{Re}}u_{yyy} \\
&\quad + \cdots + 3\tau ap_{xx} + \tau bp_{xy} - \frac{2}{3}h^2 p_{xxx} + \cdots \\
&av_x + bv_y + p_y - \frac{1}{\mathrm{Re}}(v_{xx} + v_{yy}) = a^2\tau v_{xx} + 2ab\tau v_{xy} + b^2\tau v_{yy} \\
&\quad + \frac{1}{3}\,\frac{a(-9\tau + h^2\,\mathrm{Re})}{\mathrm{Re}}v_{xxx} + \frac{1}{5}\,\frac{b(-5\tau + h^2\,\mathrm{Re})}{\mathrm{Re}}v_{xxy} \\
&\quad + \frac{1}{5}\,\frac{a(-5\tau + h^2\,\mathrm{Re})}{\mathrm{Re}}v_{xyy} + \frac{1}{3}\,\frac{b(-9\tau + h^2\,\mathrm{Re})}{\mathrm{Re}}v_{yyy} \\
&\quad + \cdots + \tau ap_{xy} + 3\tau bp_{yy} - \frac{2}{3}h^2 p_{yyy} + \cdots
\end{aligned}
$$

Type 2:

$$
\begin{aligned}
&au_x + bu_y + p_x - \frac{1}{\mathrm{Re}}(u_{xx} + u_{yy}) = a^2\tau u_{xx} + 2ab\tau u_{xy} + b^2\tau u_{yy} \\
&\quad + \frac{1}{3}\,\frac{a(-9\tau + h^2\,\mathrm{Re})}{\mathrm{Re}}u_{xxx} + \frac{1}{5}\,\frac{b(-5\tau + h^2\,\mathrm{Re})}{\mathrm{Re}}u_{xxy} \\
&\quad - \frac{1}{10}\,\frac{a(10\tau + h^2\,\mathrm{Re})}{\mathrm{Re}}u_{xyy} - \frac{1}{6}\,bh^2 u_{yyy} \\
&\quad + \cdots + 3\tau ap_{xx} + \tau bp_{xy} - \frac{2}{3}h^2 p_{xxx} - \frac{1}{2}h^2 p_{xyy} + \cdots \\
&av_x + bv_y + p_y - \frac{1}{\mathrm{Re}}(v_{xx} + v_{yy}) = a^2\tau v_{xx} + 2ab\tau v_{xy} + b^2\tau v_{yy} \\
&\quad + \frac{1}{3}\,\frac{a(-9\tau + h^2\,\mathrm{Re})}{\mathrm{Re}}v_{xxx} + \frac{1}{5}\,\frac{b(-5\tau + h^2\,\mathrm{Re})}{\mathrm{Re}}v_{xxy} \\
&\quad - \frac{1}{10}\,\frac{a(10\tau + h^2\,\mathrm{Re})}{\mathrm{Re}}v_{xyy} - \frac{1}{6}\,bh^2 v_{yyy} \\
&\quad + \cdots + \tau ap_{xy} - \frac{1}{6}h^2 p_{yyy} + \cdots
\end{aligned}
$$

Type 3:

$$
\begin{aligned}
&au_x + bu_y + p_x - \frac{1}{\mathrm{Re}}(u_{xx} + u_{yy}) = a^2\tau u_{xy} + 2ab\tau_{xy} + b^2\tau u_{yy} \\
&\quad - \frac{1}{6}\, ah^2 u_{xxx} - \frac{1}{10}\,\frac{b(10\tau + h^2\,\mathrm{Re})}{\mathrm{Re}}\, u_{xxy} \\
&\quad + \frac{1}{5}\,\frac{a(-5\tau + h^2\,\mathrm{Re})}{\mathrm{Re}}\, u_{xyy} + \frac{1}{3}\,\frac{b(-9\tau + h^2\,\mathrm{Re})}{\mathrm{Re}}\, u_{yyy} \\
&\quad + \cdots + \tau bp_{xy} - \frac{1}{6}h^2 p_{xxx} + \cdots \\
&av_x + bv_y + p_y - \frac{1}{\mathrm{Re}}(v_{xx} + v_{yy}) = a^2\tau v_{xx} + 2ab\tau v_{xy} + b^2\tau v_{yy} \\
&\quad - \frac{1}{6}ah^2 v_{xxx} - \frac{1}{10}\,\frac{b(10\tau + h^2\,\mathrm{Re})}{\mathrm{Re}}\, v_{xxy} \\
&\quad + \frac{1}{5}\,\frac{a(-5\tau + h^2\,\mathrm{Re})}{\mathrm{Re}}\, v_{xyy} + \frac{1}{3}\,\frac{b(-9\tau + h^2\,\mathrm{Re})}{\mathrm{Re}}\, v_{yyy} \\
&\quad + \cdots + \tau ap_{xy} + 3\tau bp_{yy} - \frac{1}{2}h^2 p_{xxy} - \frac{2}{3}h^2 p_{yyy} + \cdots
\end{aligned}
$$

Type 4:

$$
\begin{aligned}
&au_x + bu_y + p_x - \frac{1}{\mathrm{Re}}(u_{xx} + u_{yy}) = a^2\tau u_{xx} + 2ab\tau u_{xy} + b^2\tau u_{yy} \\
&\quad - \frac{1}{6}ah^2 u_{xxx} - \frac{1}{10}\,\frac{b(10\tau + h^2\,\mathrm{Re})}{\mathrm{Re}}\, u_{xxy} \\
&\quad - \frac{1}{10}\,\frac{a(10\tau + h^2\,\mathrm{Re})}{\mathrm{Re}}\, u_{xyy} + \frac{1}{6}bh^2 v_{yyy} \\
&\quad + \cdots + \tau bp_{xy} - \frac{1}{6}h^2 p_{xxx} - \frac{1}{2}h^2 p_{xyy} + \cdots \\
&av_x + bv_y + p_y - \frac{1}{\mathrm{Re}}(v_{xx} + v_{yy}) = a^2\tau v_{xx} + 2ab\tau v_{xy} + b^2\tau v_{yy} \\
&\quad - \frac{1}{6}ah^2 v_{xxx} - \frac{1}{10}\,\frac{b(10\tau + h^2\,\mathrm{Re})}{\mathrm{Re}}\, v_{xxy} \\
&\quad - \frac{1}{10}\,\frac{a(10\tau + h^2\,\mathrm{Re})}{\mathrm{Re}}\, v_{xyy} - \frac{1}{6}bh^2 v_{yyy} \\
&\quad + \cdots + \tau ap_{xy} - \frac{1}{2}h^2 p_{xxy} - \frac{1}{6}h^2 p_{yyy} + \cdots
\end{aligned}
$$

Thanks to the above modified equations, the consistency property is retained using the proposed streamline upwinding scheme.

5. ANALYTICAL VALIDATION

The justification for applying Eqs. (7)–(8) to obtain finite-element solutions for Eqs. (1)–(2), subject to pressure boundary conditions (9)–(10), will be presented first. As a validation study of the proposed method, we consider the Kovasznay flow

problem to obtain the rate of convergence of the finite-element method [12]. Upon specification of the boundary values in the square shown schematically in Figure 3, the exact solutions are obtained as follows:

$$u = 1 - e^{\lambda x}\cos(2\pi y) \tag{24}$$

$$v = \frac{\lambda}{2\pi} e^{\lambda x}\sin(2\pi y) \tag{25}$$

$$p = \frac{1}{2}(1 - e^{2\lambda x}) \tag{26}$$

where

$$\lambda = \frac{\mathrm{Re}}{2} - \left(\frac{\mathrm{Re}^2}{4} + 4\pi^2\right)^{1/2}$$

In this study, a remeshing procedure is used to uniformly divide the physical domain, leading to continuously refined grids with resolutions of $\Delta x = \Delta y = 1/10$, $1/20$, and $1/40$. Table 5 tabulates the L_2 error norms obtained for the case with pressure boundary condition specified at the boundary $x = 1$. For comparison purposes, results obtained for the case with prescribed velocity boundary condition have also been tabulated in Table 6. It has been shown that good agreement has been obtained with exact solutions. The legitimate use of our method to solve the problem with a specified pressure boundary condition is thus demonstrated. Also given in these tables are the rates of convergence, from which it is concluded that the present finite-element model formally provides the same spatial rate of convergence, regardless of the employed boundary conditions.

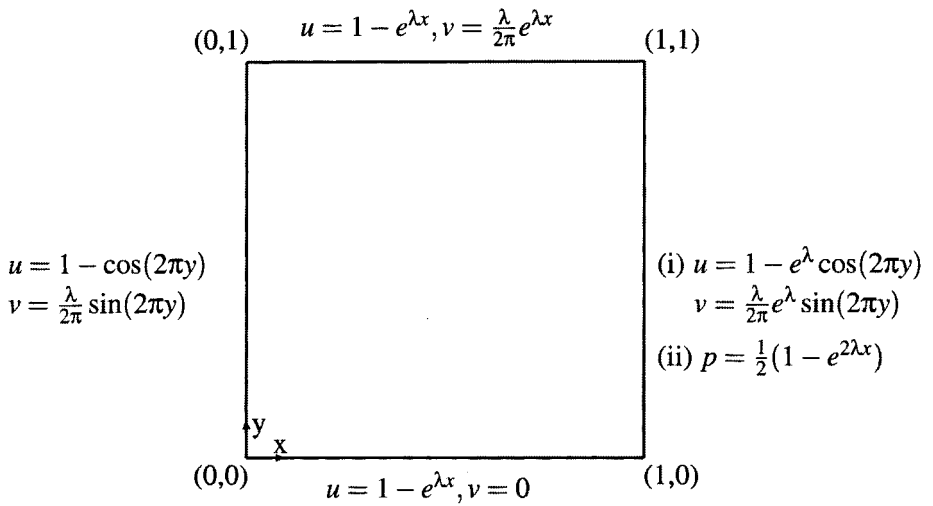

Figure 3. A schematic illustration of the boundary condition specified at the four boundaries: case (i), specify **u** at the boundary $x = 1$; case (ii), specify p at the boundary $x = 1$.

Table 5. Case with the specified Dirichlet-type velocity boundary condition

Element numbers	Velocity u	Convergence order (c)	Pressure p	Convergence order (c)
10×10	1.4194×10^{-4}		8.3611×10^{-3}	
20×20	5.1677×10^{-5}	1.46	2.2842×10^{-3}	1.87
40×40	1.7168×10^{-5}	1.59	5.9942×10^{-4}	1.93

Table 6. Case with the specified Dirichlet-type pressure boundary condition

Element numbers	Velocity u	Convergence order (c)	Pressure p	Convergence order (c)
10×10	1.4193×10^{-4}		8.3610×10^{-3}	
20×20	5.1674×10^{-5}	1.46	2.2845×10^{-3}	1.87
40×40	1.7168×10^{-5}	1.59	5.9942×10^{-4}	1.93

6. NUMERICAL RESULTS AND DISCUSSION

Backward-Facing Step Problem

The problem of interest considers a flow over a backward-facing step, shown schematically in Figure 4. The height of the entrance channel is $h = 0.9423$, and the downstream channel height is $H = 1.9423$, leading to an expansion ratio $\bar{\delta} = H/h = 2.0612$. At the entry which is sufficiently upstream of the step with a length of $l = 1.9231$, the flow profile is that of the fully developed type. Denote by $2h$ the characteristic length and the average inlet velocity by the characteristic velocity; the Reynolds number chosen for this study is 800, which falls within the laminar regime. The length of the channel is 38, which is sufficient to allow the expansion flow to fully develop again. It is thus rational to assign the Neumann-type velocity boundary condition at the channel exit. We conduct finite-element analysis for this flow condition first [8]. As revealed by Figure 5, the predicted primary reattachment length agrees well with the experimental value of 14.289 [7].

The analysis is followed by prescribing the pressure just obtained at the outlet channel. We compare two sets of computed solutions, shown in Figures 6 and 7, with the computed difference on the order of 10^{-7} for both velocities and pressure. As these figures show, results obtained under different outflow boundary conditions are essentially the same. This justifies the use of the pressure boundary condition in finite-element simulation of inflow–outflow problems.

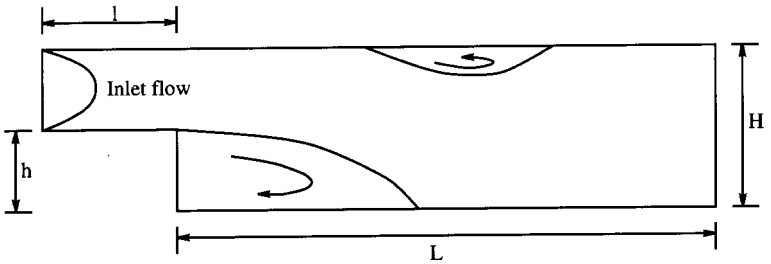

Figure 4. Schematic of the backward-facing-step problem.

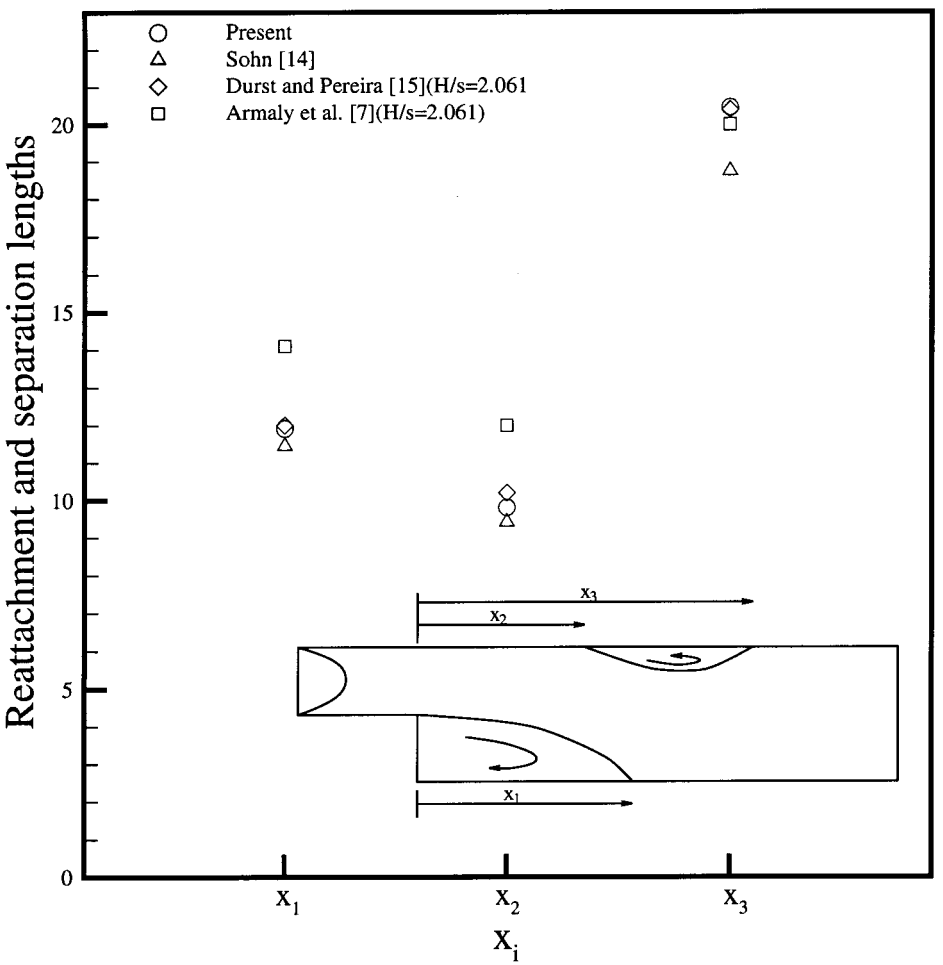

Figure 5. Comparison of the computed lengths of x_1, x_2, and x_3 with other data.

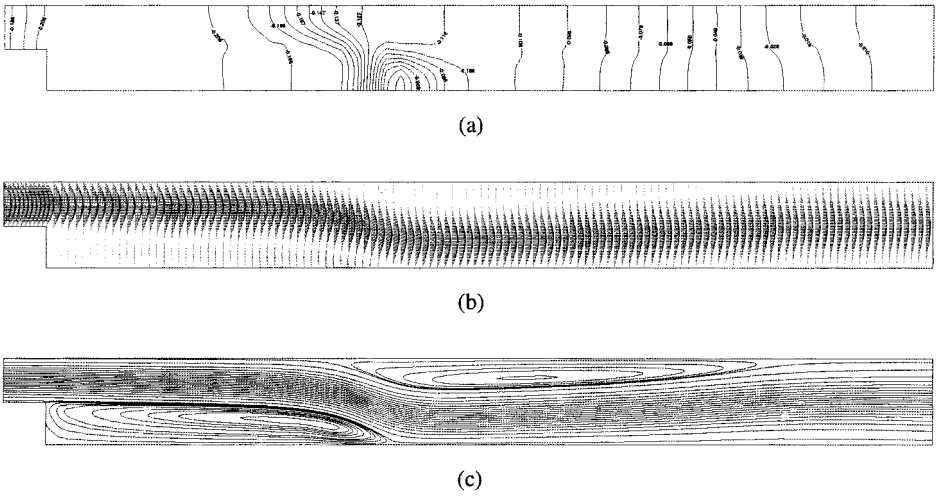

Figure 6. Computed results based on the Dirichlet-type velocity boundary conditions: (*a*) pressure contours; (*b*) velocity vector plot; (*c*) streamline plot.

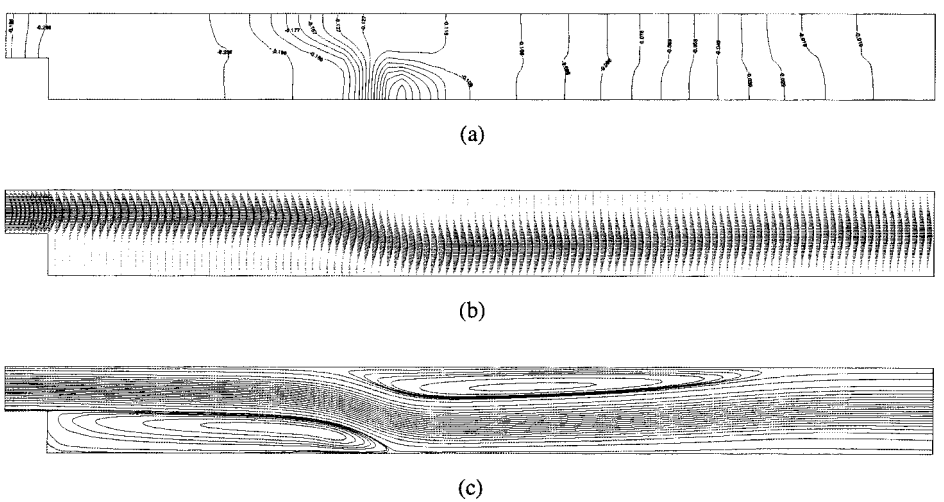

Figure 7. Computed results based on the pressure boundary conditions prescribed at the outlet: (*a*) pressure contours; (*b*) velocity vector plot; (*c*) streamline plot.

Hemodynamics in Carotid Bifurcation

Study of hemodynamics in a carotid artery is of considerable clinical importance, since atherosclerotic lesions may show their presence in the carotid sinus. Progressively, carotid bifurcation atherosclerosis can cause plaque disruption, clot formation, and, finally, a fatal stroke to occur. There is thus ample motivation to extend our knowledge of blood flow structure in the carotid artery. As a test problem, we consider steady flow in a model of the carotid bifurcation. The model geometry, shown schematically in Figure 8, is represented mathematically as follows:

$$\begin{aligned}
&\text{Curve ABC:} && \sinh[c(y-e_1)]\sinh[c(-x\sin\theta_1 + y\cos\theta_1 - s_1)] = h_1\\
&\text{Curve GHI:} && \sinh[c(y+e_2)]\sinh[c(x\sin\theta_2 + y\cos\theta_2 + s_2)] = h_2\\
&\text{Curve DEF:} && \sinh[c(-x\sin\theta_1 + y\cos\theta_1 + s_1)]\\
& && \quad\times \sinh[c(x\sin\theta_2 + y\cos\theta_2 - s_2)] = h_3
\end{aligned} \tag{27}$$

The parameters for defining the model vessel configuration are as follows: $h_1 = 0.0365$, $h_2 = 0.0927$, $h_3 = 0.0019$, $l_0 = 4$, $l_1 = 12$, $l_2 = 12$, $c = 3$, $d_1 = 0.29$, $d_2 = 0.0345$, $\theta_1 = 25.1°$, $e_1 = 0.4$, $V_1 = 0.055$, $\theta_2 = 25.4°$, $e_2 = 0.6$, $V_2 = 0.21$, $w_1 = 1.00$, $w_2 = 1.23$, $p_1 = 0.964$, and $p_2 = 1.790$. Another control parameter s_j is that of $(j = 1{-}2)$ which is given by $s_j = d_j + V_j \operatorname{sech}[z(1 + 0.3z^4)]$, where $z = [x\cos\theta_j - (-1)^j y\sin\theta_j - p_j]/w_j$.

To resolve the blood flow in sufficient detail, grids should be clustered in regions of high gradient solutions. Figure 9 shows the finite-element mesh, which

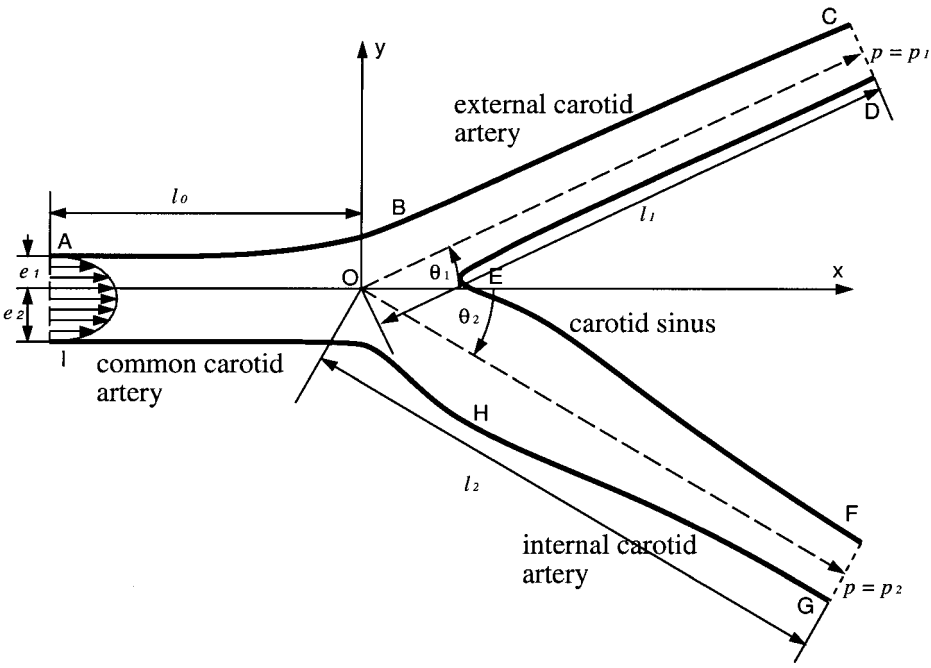

Figure 8. Schematic of the bifurcation blood problem.

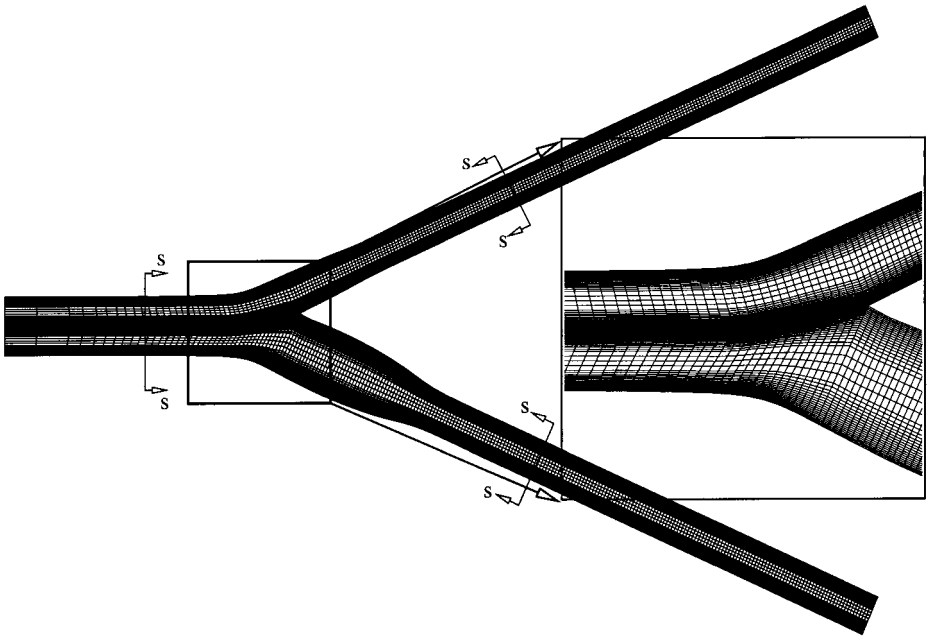

Figure 9. Finite-element mesh used for the hemodynamic analysis. Grid details are also shown in the bifurcation region.

involves 19,721 nodal points and 4,800 biquadratic elements. A close-up view of the mesh in the regions of bifurcation is also included to address its importance. For the sake of brevity, a fully developed steady entry flow was specified in the common carotid artery. Constant pressures were specified at the outlets of the internal and external carotid arteries, respectively. In this study, we considered three different pressure differences ($\Delta p \equiv p_2 - p_1$), namely, 0, -5, 5, to reveal the influence of Δp on the flow development in the artery. Under the rigid vessel wall assumption, the no-slip boundary condition was applied there.

The calculation was performed at $\mathrm{Re} = 100$, which was defined using $(e_1 + e_2)$ as the reference length, while u_{mean} was used as the characteristic velocity. While $150 \leq \mathrm{Re} \leq 600$ is typical for blood flow analysis, we considered a low Reynolds number case in the present study mainly for comparison purposes [9]. Figure 10 depicts the velocity profiles and Figure 11 plots the streamline contours showing the flow reversal along the outer wall of the carotid sinus. The carotid region is enlarged immediately downstream of the bifurcation. The region of slow blood flow is precisely the region where plaque localizes. The rationale for this is that the outer wall of the carotid sinusis an area of low wall shear stress, as revealed by Figure 12. According to Ku et al. [10] and Zarins et al. [11], low shear stress is one of the major risk factors leading to vascular disease.

We also compare the computed wall shear stress, defined by $\mu\, \partial u_t / \partial n$, with that of Hunt for the case $\Delta p = 0$ [9]. Figure 13 reveals good agreement between the two sets of data. We also plot wall shear stresses computed under $\Delta p = 5$ and -5 at

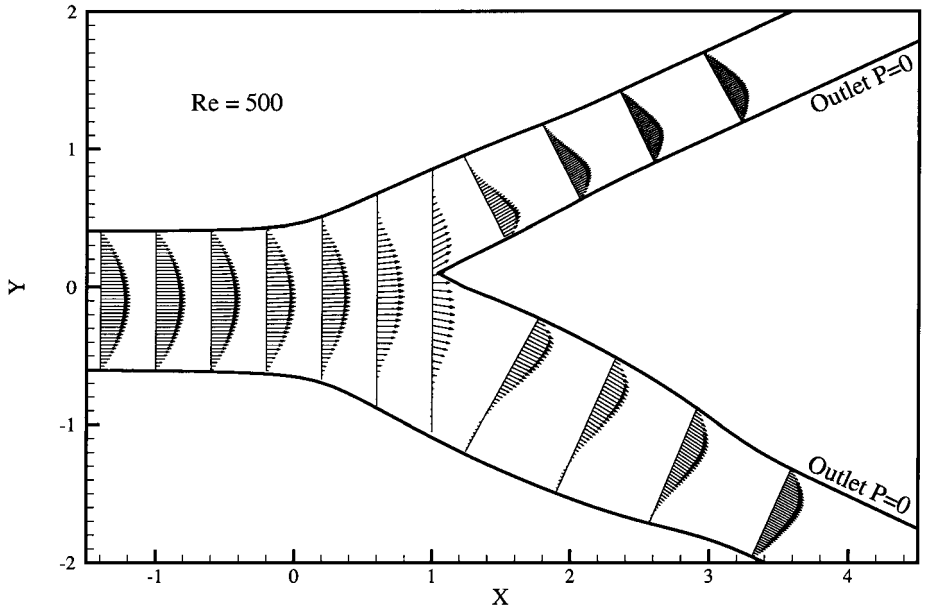

Figure 10. Velocity profiles plotted at several selected locatoins for the case of Re = 500.

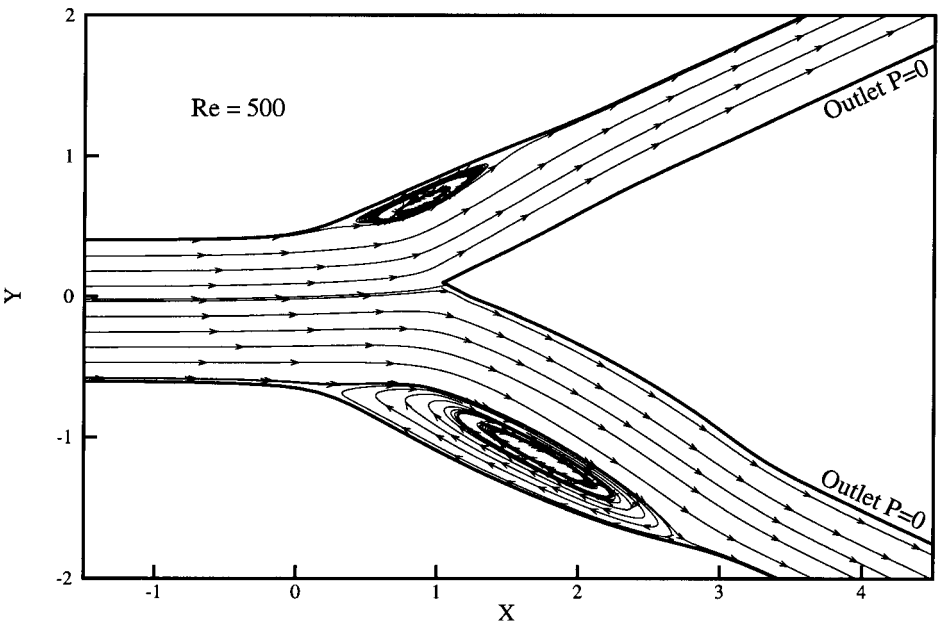

Figure 11. Streamline contours for the case of Re = 500 for showing flow recirculation in the artery.

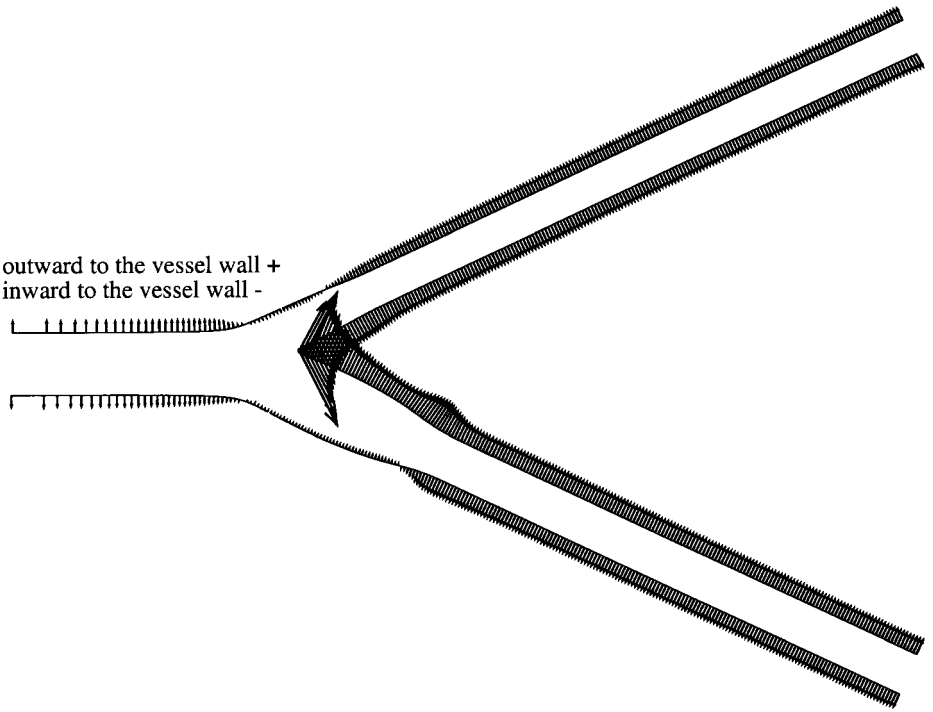

Figure 12. Shear stress distribution along the vessel wall for the case with $Re = 500$.

$Re = 100$ in Figures 14 and 15, respectively, to show that the prescribed outlet pressure can affect the hemodynamic performance. To show the effect of the end pressure on the flow pattern, we plot in Figure 16 the pressure contours and in Figure 17 the streamlines for $Re = 100$. Depending on the difference of two end pressures, different degrees of flow reversal will result.

7. CONCLUDING REMARKS

In this study, a streamline upwind finite-element method has been developed on biquadratic elements to simulate incompressible viscous flows. It has been emphasized that the pressure boundary condition is specified theoretically. Results of two benchmark tests compare favorably with those obtained subject to Dirichlet-type velocity conditions, thus showing the validity of the algorithm presented here. We have also applied the computationally efficient mixed finite-element code to simulate hemodynamics in carotid bifurcation. Different values of outlet pressure are considered to study their influence on the flow development in the artery.

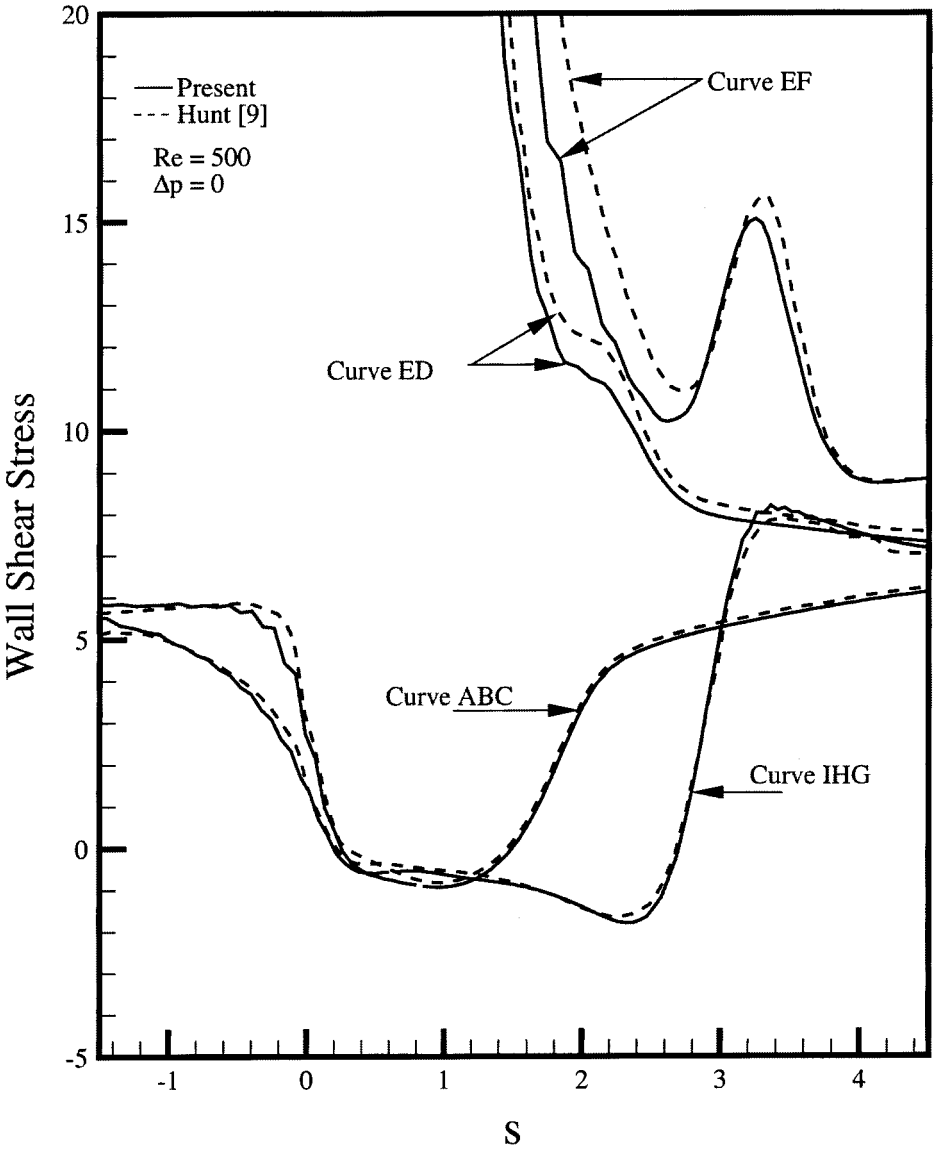

Figure 13. Comparison of wall shear stresses, plotted against s defined in Figure 9, with those computed by Hunt for the case at $\mathrm{Re} = 500$ and $\Delta p = 0$.

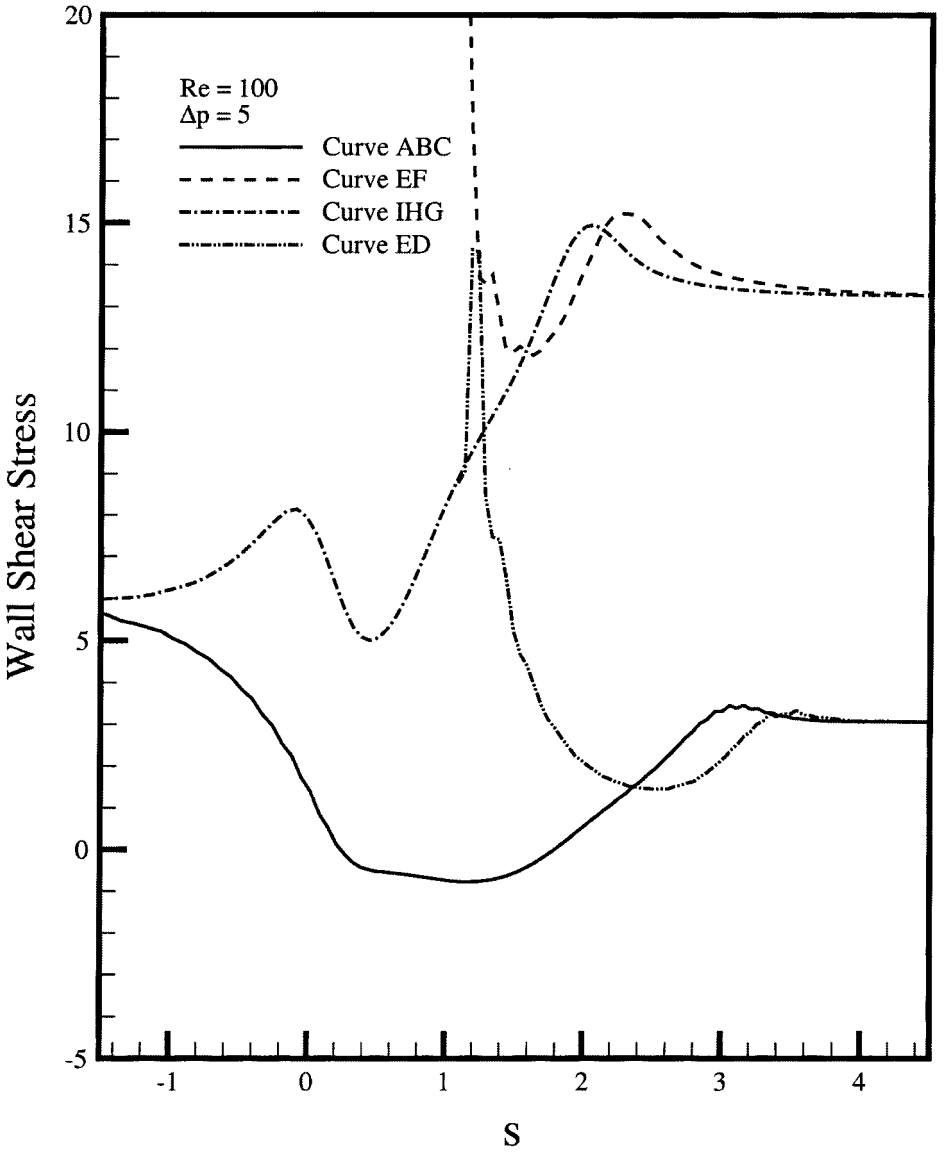

Figure 14. Plot of wall shear stresses against s defined in Figure 9 for the case at $\mathrm{Re} = 100$ and $\Delta p = 5$.

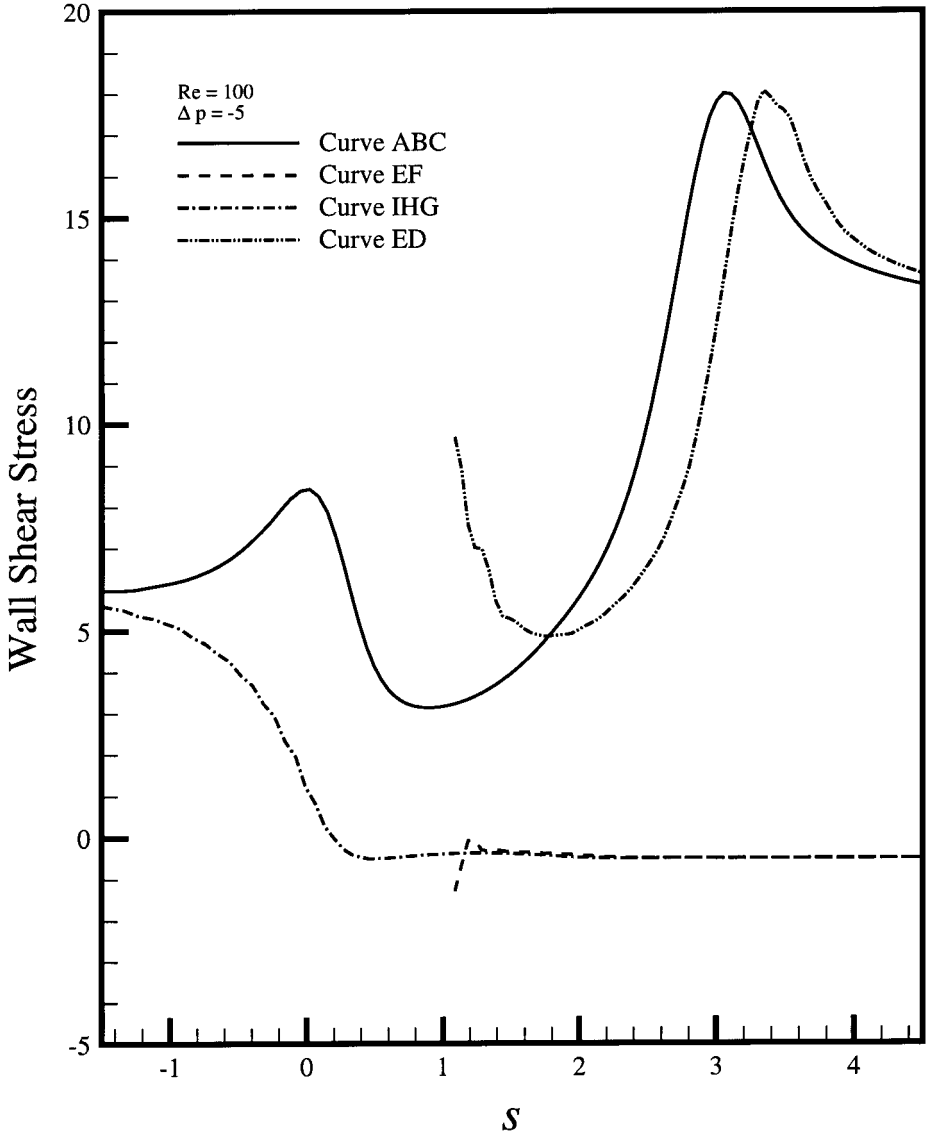

Figure 15. Plot of wall shear stresses against s defined in Figure 9 for the case at Re $= 100$ and $\Delta p = -5$.

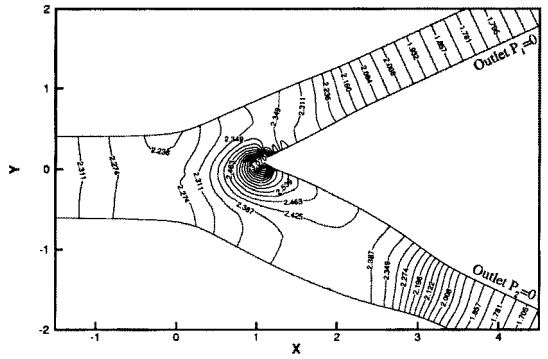

(a)

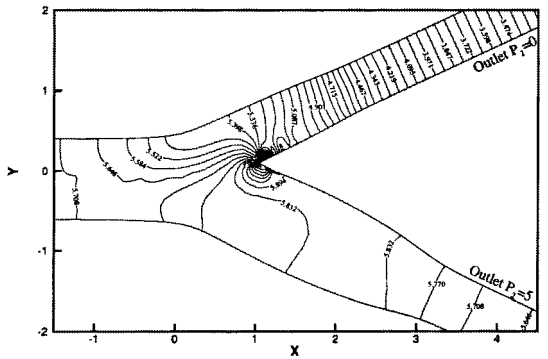

(b)

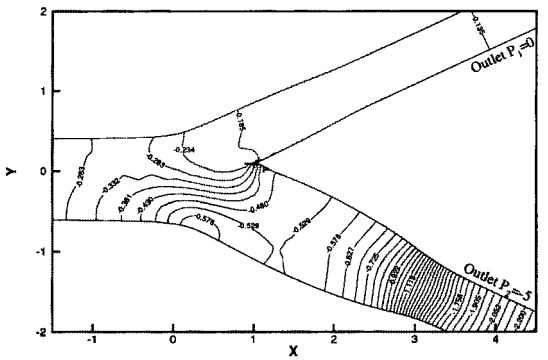

(c)

Figure 16. Pressure contours for the case with Re = 100: (*a*) $p_2 - p_1 = 0$; (*b*) $p_2 - p_1 = 5$; (*c*) $p_2 - p_1 = -5$.

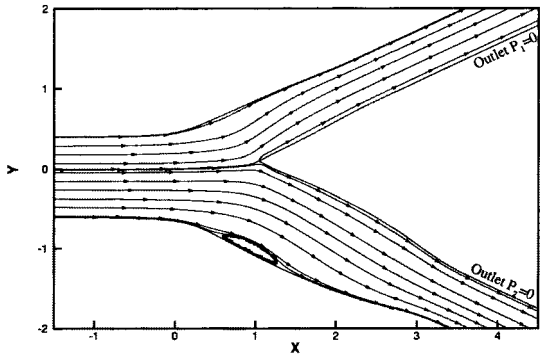

(a)

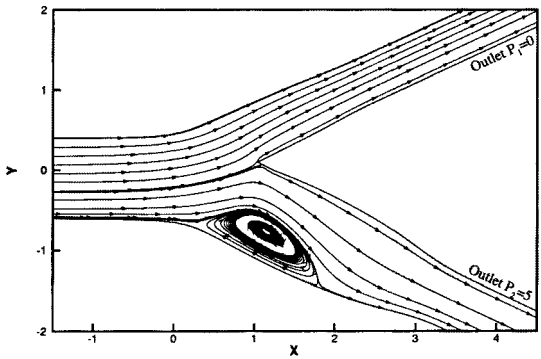

(b)

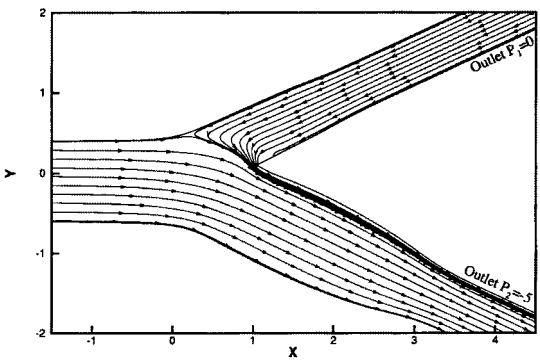

(c)

Figure 17. Streamline plots for the case with Re = 100: (*a*) $p_2 - p_1 = 0$; (*b*) $p_2 - p_1 = 5$; (*c*) $p_2 - p_1 = -5$.

REFERENCES

1. M. D. Gunzburger, *Finite Element Methods for Viscous Incompressible Flows, A Guide to Theory, Practice, and Algorithms*, Academic Press, London, 1989.
2. L. Quartapelle, *Numerical Solution of the Incompressible Navier–Stokes Equations*, Birkhäuser Verlag, Basel, Switzerland, 1993.
3. T. J. R. Hughes and A. Brooks, A Multi-dimensional Upwind Scheme with No Crosswind Diffusion, in T. J. R. Hughes (ed.), *Finite Element Methods for Convection Dominated Flows*, AMD Vol. 34, ASME, New York, 1979.
4. F. Brezzi and J. Douglas, Stabilized Mixed Methods for the Stokes Problem, *Numer. Math.*, vol. 53, pp. 225–235, 1988.
5. I. Babuška, Error Bounds for Finite Element Methods, *Numer. Math.*, vol. 16, pp. 322–333, 1971.
6. T. W. H. Sheu, S. F. Tsai, and M. M. T. Wang, A Petrov–Galerkin Formulation for Incompressible Flows at High Reynolds Numbers, *J. Comput. Fluid Dyn.*, vol. 5, pp. 213–230, 1995.
7. B. F. Armaly, F. Durst, J. C. F. Pereira, and B. Schonung, Experimental and Theoretical Investigation of Backward-Facing Step Flow, *J. Fluid Mech.*, vol. 127, pp. 473–496, 1983.
8. M. T. Wang and Tony W. H. Sheu, Implementation of a Free Boundary Condition to Navier–Stokes Equations, *Int. J. Numer. Meth. Heat & Fluid Flow*, vol. 7, no. 1, pp. 95–111, 1997.
9. R. Hunt, The Numerical Solution of the Flow in a General Bifurcating Channel at Moderately High Reynolds Number Using Boundary-Fitted Co-ordinates, Primitive Variables and Newton Iteration, *Int. J. Numer. Meth. Fluids*, vol. 17, pp. 711–729, 1993.
10. D. N. Ku, D. P. Giddens, C. K. Zarins, and S. Glagov, Pulsatile Flow and Atherosclererosis in the Human Carotid Bifurcation, Postive Correlation between Plaque Location and Low Oscillating Shear Stress, *Arteriosclerosis*, vol. 5, pp. 293–302, 1985.
11. C. K. Zarins, D. P. Giddens, B. K. Bharadvaj, V. S. Sottiurai, R. F. Mabon, and S. Glagov, Carotid Bifurcation Atherosclerosis: Quantitative Correlation of Plaque Localization with Flow Velocity Profiles and Wall Shear Stress, *Circulation Res.*, vol. 53, pp. 502–514, 1983.
12. L. S. G. Kovasznay, Laminar Flow Behind a Two Dimensional Grid, *Proc. Camb. Phil. Soc.*, vol. 44, pp. 58–62, 1948.
13. D. W. Pepper and A. J. Baker, Finite Differences versus Finite Elements, in W. J. Minkowycz et al. (eds.), *Handbook of Numerical Heat Transfer*, pp. 519–577, Wiley, New York, 1988.
14. J. L. Sohn, Evaluation of FIDAP on Some Classical Laminar and Turbulent Benchmarks, *Int. J. Numer. Meth. Fluids*, vol. 8, pp. 1469–1490, 1988.
15. F. Durst and J. C. F. Pereira, Time-Dependent Laminar Backward-Facing Step Flow in a Two-Dimensional Duct, *J. Fluids Eng.*, vol. 110, pp. 289–296, 1988.